Journal of the European Ceramic Society 21 (2001) 2569–2576

www.elsevier.com/locate/jeurceramsoc

Elastic constants of mullite containing alumina platelets

H. Ledbetter[a,*], S. Kim[a], M. Dunn[b], Z. Xu[c], S. Crudele[c], W. Kriven[c]

[a]National Institute of Standards and Technology, Boulder, CO, USA
[b]Department of Mechanical Engineering, University of Colorado, Boulder, CO, USA
[c]Department of Materials Science and Engineering, University of Illinois, Urbana, IL, USA

Abstract

Using dynamic methods, we measured the elastic constants of a composite comprising alumina platelets (0.2 volume fraction) in a 3:2 mullite matrix. Instead of the expected elastic stiffening, we found an elastic softening. For example, the Young modulus was 222 GPa, below mullite's value of 228 GPa, and far below the value predicted by a solid-mechanics model assuming good alumina–mullite interfaces: 256 GPa. As possible softening sources, we considered voids, cracks, poor particle–matrix-interface bonding, and an enveloping third phase, either around the platelets or around the mullite particles. We concluded that the mullite particles must be enveloped by silica, an elastically soft phase. Solid-mechanics modeling considering a three-phase composite supports our conjecture. Our conjecture received further confirmation from careful SEM and STEM observations.

Keywords: Composites; Elastic constants; Internal friction; Mullite; Platelets

1. Introduction

Mullite's processing, properties, and applications are well reviewed.[1] Mullite, of nominal composition $3Al_2O_3{\cdot}2SiO_2$, is a highly attractive candidate for oxide composites. As a matrix, it is a widespread 'workhorse' refractory material, having good creep resistance and chemical stability up to 1600°C. The current, widely accepted phase diagram indicates that the equilibrium phase grown by solid-state reaction has a narrow solid-solution range around the $3Al_2O_3{\cdot}2SiO_2$ (abbreviated 3:2) composition.[2] Applications of mullite composites range from electronic-packaging materials to jet-engine linings. Principal hopes for particle-reinforced mullite are higher flexural strength and higher toughness in more diverse shapes.

Studying a material's elastic constants offers several advantages: (1) elastic constants allow accurate measurement (1 part in 1000 is easy); (2) elastic constants provide a valuable probe of microstructure: particle volume fraction and shape, heterogeneities, internal stresses, texture, others; (3) elastic constants often correlate either theoretically or empirically with other physical properties and even with mechanical-deformation properties.

Internal friction Q^{-1} is the imaginary part of the total elastic constant

$$\tilde{C} = C + iC'' = C(1 + iQ^{-1}). \tag{1}$$

or

$$Q^{-1} = C''/C, \tag{2}$$

the ratio of the real to imaginary parts. Internal friction is extremely sensitive to material defects, any defect varying from phonons to cracks. Any measurement of C yields also the accompanying Q^{-1}.

2. Materials

The mullite powder for the matrix was KM mullite-101 (Kyoritsu, Nagoya, Japan). (We use trade names to characterize the studied material and permit reproduction of our results. They are not endorsements of particular products. Other products might function as well or better.) X-ray diffraction and fluorescence confirmed the 3:2 composition. The particle-size distribution determined by sedigraphy was 0 to 2 μm with a mean size of 0.84 μm.

Alumina platelets were obtained from Du Pont (E.I. du Pont de Nemours & Co., Central Research and Development Experimental Station, Wilmington, Delaware). Each platelet was a monocrystal. Because of the alumina crystals' symmetry (trigonal, $R\bar{3}c$), they possessed roughly hexagonal shapes. The size and density of the alumina platelets and the mullite are given in

* Corresponding author. Fax: +1-303-497-5030.
E-mail address: ledbetter@boulder.nist.gov (H. Ledbetter).

0955-2219/01/$ - see front matter
PII: S0955-2219(01)00269-2

Table 1. Scanning electron micrographs indicated that the platelets were 2 to 5 μm thick (Fig. 1).

The composites were processed by mixing alumina platelets (0.2 volume fraction) and mullite powder (0.8 volume fraction). The mixture was shear-homogenized for 2 min in hexane containing 0.1 volume fraction of the solids. A high-shear-rate homogenizer was used. The batch was dried overnight at about 100°C and sieve-granulated with a 250-μm screen. Granulated batches were hot-pressed for 1 h at 34.5 MPa (5000 psi) at temperatures between 1500 and 1600°C to produce cylinders about 1 cm thick and several cm in diameter. The cylinders were black because graphite die and plungers and the vacuum atmosphere made them slightly oxygen deficient. A representative microstructure is shown in Fig. 2. Three specimens were examined; their processing parameters are summarized in Table 2.

3. Measurements

To measure the elastic constants C and the internal friction Q^{-1}, we used acoustic-resonance spectroscopy.[3–5] The method offers numerous advantages.[6] These include (1) a single small specimen, (2) no bonding agent (contactless), except at two points, (3) a single frequency sweep to get the entire elastic-stiffness tensor C (even for the lowest symmetry), (4) low inaccuracy (typically 1 in 1000 or better), (5) simultaneous Q^{-1} measurements, thus the full internal-friction tensor Q^{-1}. Fig. 3 shows a vibration-frequency spectrum. Despite its complexity, the material yields sharp mechanical-resonance peaks.

Table 1
Physical properties of alumina platelets and mullite powder

Material	Density[a] (g/cm³)	Surface area[b] (m²/g)	Diameter (μm)
Alumina platelets (batch A)	3.94	1.3	1–8 (mean: 5)
Alumina platelets (batch B)	3.98	0.13	20–80 (mean: 40)
Kyoritsu mullite	3.12	29.4	0.84 (mean)

[a] Helium pycnometry.
[b] BET.

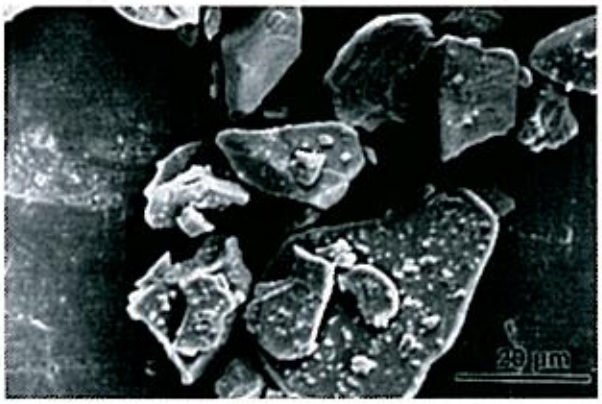

Fig. 1. SEM image of alumina platelets showing rounded triangular–hexagonal symmetry, which reflects the rhombohedral crystal structure. Batch A.

4. Results and discussion

Table 3 gives the measured C for an assumed general orthorhombic symmetry. First, we note that the material is slightly anisotropic: $2C_{66}/(C_{44}+C_{55})=1.04$, instead of unity, as required for isotropy. We assume this anisotropy arises from the nonrandom distribution of platelet orientations. Because alumina is stiffer than mullite, alumina platelets oriented preferentially perpendicular to the pressing direction x_3 would cause $C_{66} > C_{44}=C_{55}$, $C_{33} < C_{11}=C_{22}$, $E_{33} < E_{11}=E_{22}$, $\nu_{31} > \nu_{13}$, where E denotes Young modulus and ν the Poisson ratio. The measurements meet all these conditions.

At the bottom of Table 3, we give the Voigt–Reuss–Hill averaged-over-direction quasi-isotropic elastic constants.

The internal-friction Q^{-1} results show some interesting features. First, we note the exceptionally low values for

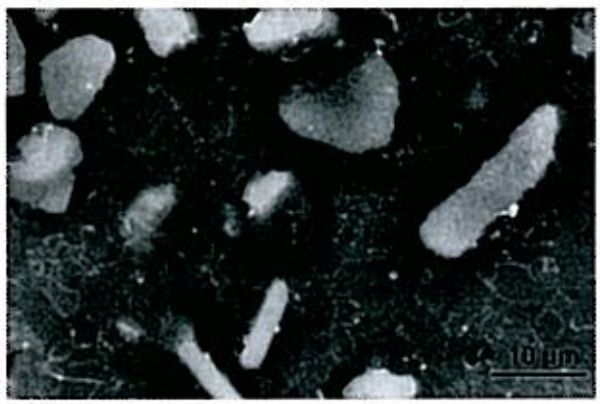

Fig. 2. SEM image of alumina platelets (batch A) in mullite after hot-pressing and thermal etching at 1400°C for 1 h. Standard secondary-electron image. This image fails to reveal an observed tendency of the platelets to align perpendicular to the hot-press stress axis.

Table 2
Composite processing parameters

Composite no.	Platelet diameter (μm)	Hot-press conditions	
		Temperature (°C)	Pressure (MPa)
3	40	1550	34.5
4	40	1500	34.5
8	5	1500	34.5

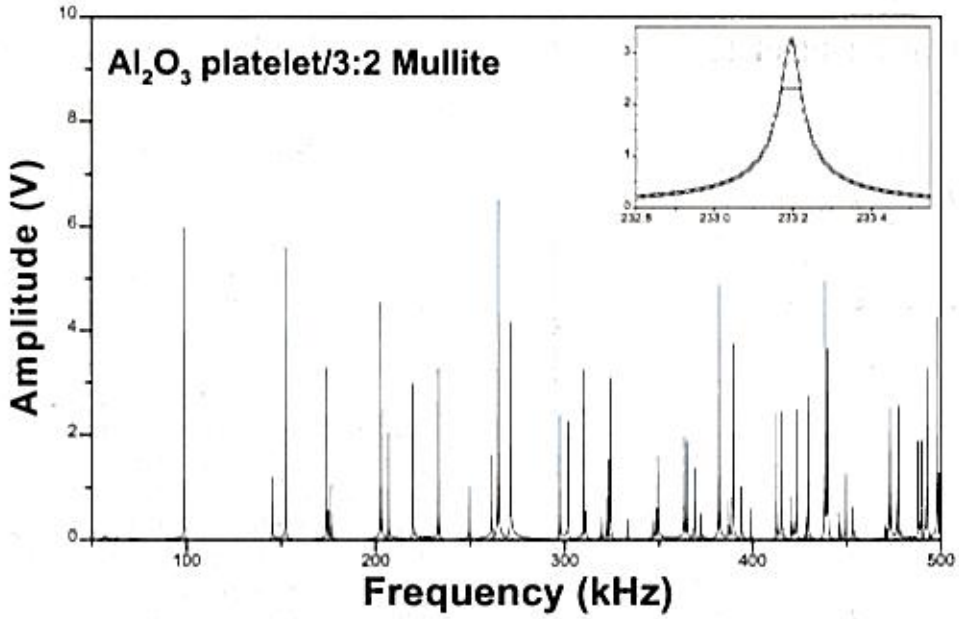

Fig. 3. Vibration-frequency spectrum. Resonance-peak frequencies give elastic stiffnesses. Peak widths give internal frictions.

Q^{-1} corresponding to C_{33} and E_{33}. Both of these deformation modes contain a large extensional–compressional component in the x_3 direction. One explanation for the low values is that the platelet–matrix interfacial bonding is much stronger along x_3 than along x_1 and x_2, a reasonable hypothesis considering the platelet geometry. (Bonding at platelet surfaces exceeds that at edges.) Second, we note the relative values of $Q_G{}^{-1}$ and $Q_{CL}{}^{-1}$. (Subscripts G and C_L indicate shear and longitudinal modes, respectively.) If most of Q^{-1} arises from phonons, theory[7] predicts $Q_G{}^{-1}/Q_{CL}{}^{-1} = 3$, versus the observed ratio 0.43/0.30 = 1.4. Some other defect must be increasing $Q_{CL}{}^{-1}$. Again, weaker bonding at platelet edges offers a possible explanation.

The most surprising result in Table 3 is the generally low measured C values. Beside the measurements, Table 3 contains values predicted by a wave-scattering model,[8] a model tested successfully[9] for various particle-reinforced composites and yielding measurement–theory agreement within a few percent or better. Also, we verified that this model gives the same results as the extended Mori–Tanaka model described elsewhere[10] and below. For the calculations, we took the 3:2 mullite values reported by Ledbetter and co-workers[11] and the alumina elastic constants reported by Tefft[12] (Table 4). Fig. 4 illustrates the situation for the Young modulus.

Table 3
Elastic properties of a mullite-matrix composite containing 0.2 volume fraction of alumina platelets[a]

	Measurement		Theory
	C_{ij} (GPa)	$Q_{ij}^{-1}(10^{-3})$	C_{ij} (GPa)
C_{11}	273.52	0.28	325
C_{22}	275.39	0.87	325
C_{33}	256.33	0.07	325
C_{44}	87.428	0.23	98.2
C_{55}	87.186	0.32	98.2
C_{66}	90.606	0.25	101
C_{12}	92.622		123
C_{13}	91.536		116
C_{23}	89.155		116
B	150.12	0.20	187
E_{11}	225.71	0.46	260
E_{22}	229.04	1.19	260
E_{33}	211.84	0.11	265
ν_{12}	0.24873		0.288
ν_{21}	0.25240		0.288
ν_{13}	0.27059		0.254
ν_{23}	0.25768		0.254
ν_{31}	0.25396		0.259
ν_{32}	0.23832		0.259
ρ (g/cm^3)	3.2792		
C_L	268.08	0.30	322
G	88.473	0.43	111
E	221.84	0.39	256
ν	0.25371		0.272

[a] Alumina platelets aspect ratio = 40:1.5 (40 μm diameter and 1–2 μm thick); ν_{ij} are dimensionless.

Table 4
Elastic properties of three constituents

	Mullite	Silica	Alumina
C_L (GPa)	293.2	87.81	467.7
G (GPa)	89.47	35.54	161.7
B (GPa)	173.9	40.44	252.1
E (GPa)	229.1	82.45	399.6
ν	0.2804	0.1600	0.2358

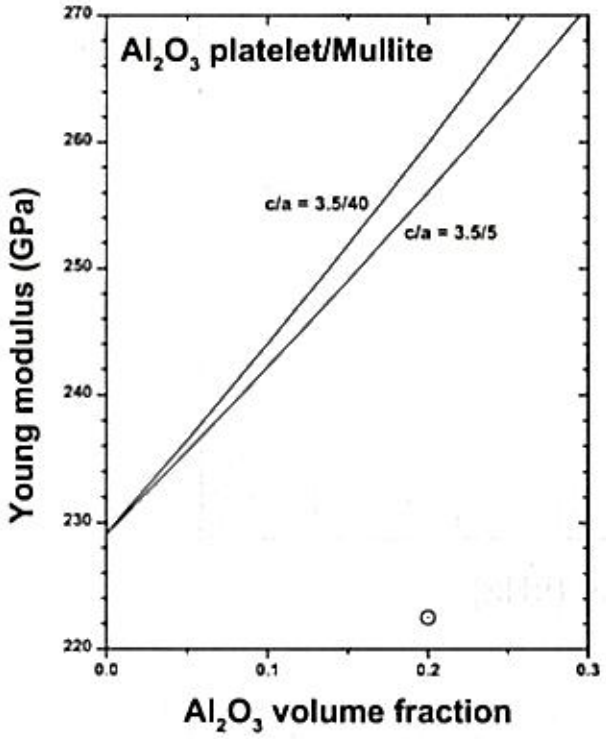

Fig. 4. Young modulus calculated for two particle sizes. Circle near bottom indicates measurement.

The measurement falls below that of pure mullite and well below theoretical prediction.

Elastic softening can arise from several sources:

1. voids
2. cracks
3. poor particle-interface bonding
4. enveloping soft phase around particles
5. enveloping soft phase around matrix particles.

As the softening source, voids are easiest to exclude because the material shows near-theoretical mass density, and 11% voids are required to lower the Young modulus by 15%. We exclude cracks for two reasons: (1) neither SEM nor TEM revealed a significant crack density; (2) theory[13] shows that the required crack density would lower the Poisson ratio to a value much lower than observed. We would expect excellent alumina–mullite interfaces because the two materials are similar in chemical composition and bonding type (ionic). As for a soft phase enveloping the alumina platelets, we studied this by using the solid-mechanics model described below. Using the stiffnesses in Table 4, we found that such a phase geometry cannot effect the observed elastic softening.

Thus, from the above list, we are left with only possibility 5: an enveloping phase surrounding the mullite particles. We considered this possibility.

An idealized microstructure of the alumina–mullite composite is envisioned for modeling purposes, as shown in Fig. 5. It consists of an aggregate of mullite grains, each surrounded by a thin silica shell representing the silica-rich grain boundaries. The volume fraction of the mullite grains and the silica shells are denoted by c_M and c_S. Embedded in this aggregate are alumina particles with volume fraction c_A. The volume fractions of these three phases satisfy $c_A + c_M + c_S = 1$. The mullite grains are assumed to be isotropic and spherical, as are the silica shells. Consistent with the microstructure (Fig. 1), the alumina particles are assumed to be oblate spheroids with an aspect ratio denoted by α. They are assumed to be aligned with the unique axis of the spheroid coinciding with the specimen x_3-axis, as shown in Fig. 5. While aligned, the alumina particles are assumed to be randomly oriented about the x_3-axis so that the composite exhibits transverse isotropy, with the x_1–x_2 plane as the isotropic plane. We use a hexagonal-symmetry average of the alumina monocrystal elastic moduli; elastic moduli used in the calculations for all three phases are given in Table 4.

To calculate the elastic moduli of the heterogeneous microstructure shown in Fig. 5, we use a two-step averaging approach. In the first step, we compute the effective moduli of a mullite polycrystal containing silica-rich grain boundaries. In the second step, we use the results of the first step as the matrix in a composite that is reinforced with the aligned particles. For the first step, we use the micromechanics model of Dunn and Ledbetter.[10] That model can be applied to compute the elastic moduli of a matrix phase containing arbitrary ellipsoid-shaped particles that are surrounded by a coating also of arbitrary ellipsoid shape, but which may

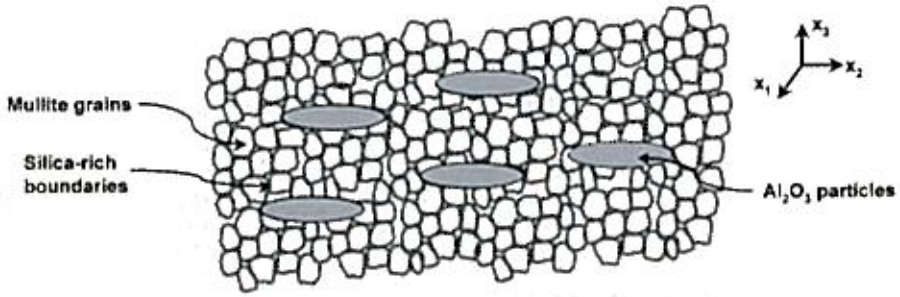

Fig. 5. Model material used for solid-mechanics calculations of effective elastic stiffnesses.

differ from the particle shape. We apply that model by assuming both the particles and matrix have properties of the mullite grains, and the silica-rich shell has properties of silica, as given in Table 4. Complete details regarding the calculation procedure are given by Dunn and Ledbetter.[10] The resulting elastic moduli of the mullite polycrystal with silica-rich grain boundaries are shown in Fig. 6 at an alumina volume fraction of zero.

The second step of the averaging approach consists of estimating the moduli of a two-phase composite consisting of alumina particles in the matrix of mullite with silica-rich grain boundaries, the moduli of which were determined in the first step. The effective elastic moduli C of the two-phase composite can be expressed exactly in terms of strain-concentration factors as

$$C = c_0 C_0 A_0 + c_1 C_1 A_1 = C_0 + c_1 (C_1 - C_0) A_1. \quad (3)$$

(see, for example, Hill[14] and Dvorak.[15]) In Eq. (3), C_i and c_i denote the elastic-stiffness tensor and the volume fraction of the ith phase, and A_i the strain-concentration factors for the ith phase where $i=0,1$ denote the matrix and particle phases, respectively. Bold symbols are used for tensorial quantities. Physically, the strain-concentration factors relate the average strain in the ith phase to the uniform srain that would be developed in a homogeneous material if it were subjected to displacement boundary conditions. In other words, $\epsilon_i = A_i \epsilon^0$ $(i=0,1)$, where ϵ^0 is the uniform strain consistent with the applied displacements. The second right-hand side is obtained by using the identities $c_0 + c_1 = 1$ and $c_0 A_0 + c_1 A_1 = I$. As is apparent from Eq. (3), the key to predicting the effective moduli of the composite is estimating the concentration factors A_i.

Here we use the Mori–Tanaka mean-field theory[16] to estimate A_i. The physical interpretation of the theory is that, when subjected to uniform-stress boundary conditions, the average stress in each fiber is equal to the average stress in a single fiber embedded in an infinite matrix subjected to a uniform far-field stress equal to the (as yet unknown) average stress in the composite. Mathematically, this assumption can be written as

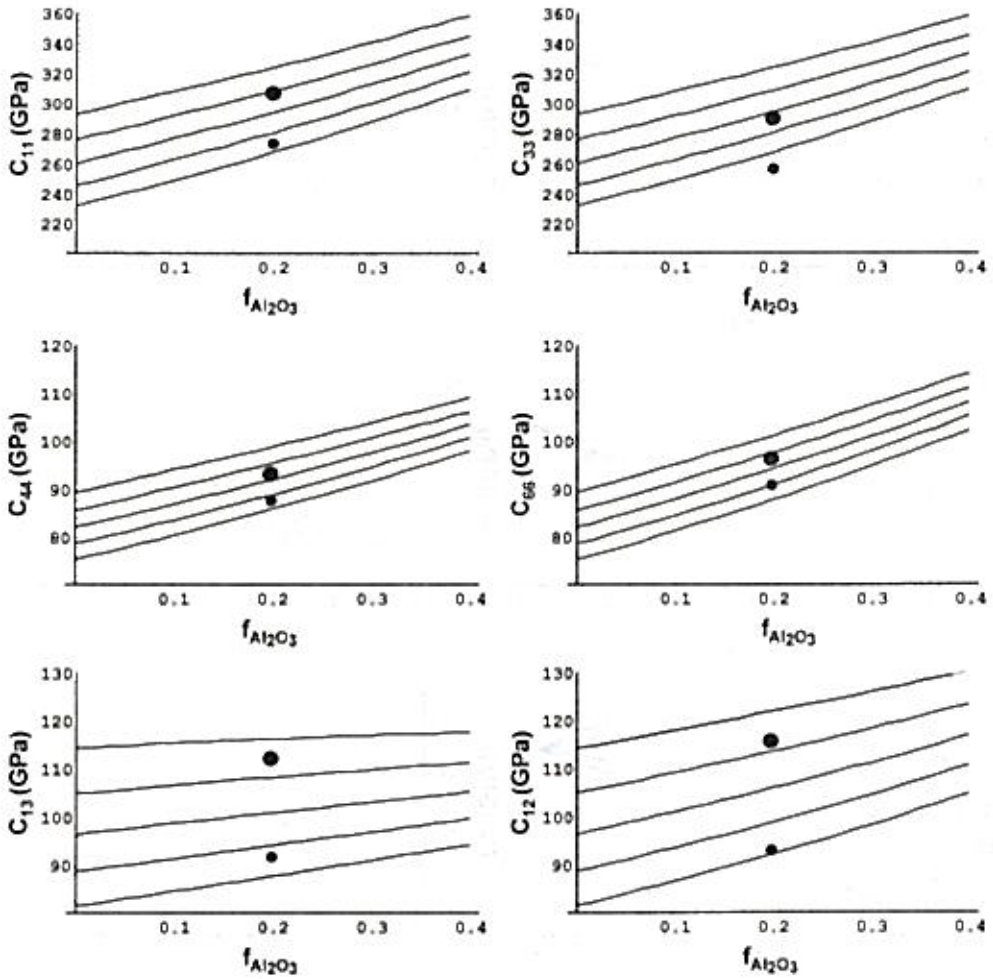

Fig. 6. Elastic stiffnesses C_0 predicted from the solid-mechanics theory described in the text. Filled circles show measurements. Curves from top to bottom correspond to various silica volume fractions: 0, 0.05, 0.10, 0.15, 0.20.

$$A_i = A^{\mathrm{dil}}\left[c_1 I + c_2 A^{\mathrm{dil}}\right]^{-1}. \quad (4)$$

$$A^{\mathrm{dil}} = \left[I + SC_0^{-1}(C_i - C_0)\right]^{-1}. \quad (5)$$

In Eqs. (4) and (5), A^{dil} denotes the concentration factor for a single particle of phase i embedded in an infinite matrix subjected to uniform far-field stress or strain boundary conditions; it is called the dilute concentration factor. It is easily determined analytically by using Eshelby's equivalent inclusion method (Eshelby,[17] Mura[18]). The effect of the particle shape is contained in the Eshelby tensor S, which is a function of the particle shape and the Poisson ratio ν of the isotropic matrix.

We carried out calculations as described above for the alumina–mullite composites as a function of alumina volume fraction. These results are shown in Fig. 6. For each component of the effective moduli C_{ij} versus alumina volume fraction, five curves are shown. These curves are calculations for various volume fractions of silica surrounding the mullite grain boundaries, ranging from 0.0 to 0.2. Also shown as solid circles are the measured components of the elastic stiffnesses of two specimens with an alumina volume fraction of 0.2.

In addition, we carried out a second set of calculations to explore the possibility that the particles, instead of the individual grains, were surrounded by a thin silica shell. These calculations were also done by using the model of Dunn and Ledbetter,[10] but in a slightly different way. The calculations showed that unrealistically high volumes of silica were required for the predictions to agree with measurements, and, furthermore, that very different volume fractions were required for each component of the effective moduli. This suggests that silica-rich regions surrounding the particles are not responsible for the observed behavior of the elastic moduli.

Fig. 6 shows the model-calculation results together with measurements on two composites. (Table 3 shows results only for the softer material.) The curves represent different volume fractions of silica (0, 0.05, 0.10, 0.15, 0.20) enveloping the mullite particles. For the softest material, about 0.15 to 0.20 volume fraction of silica is required to effect softening. For the stiffer material, about 0.05 to 0.10 is required. That almost the

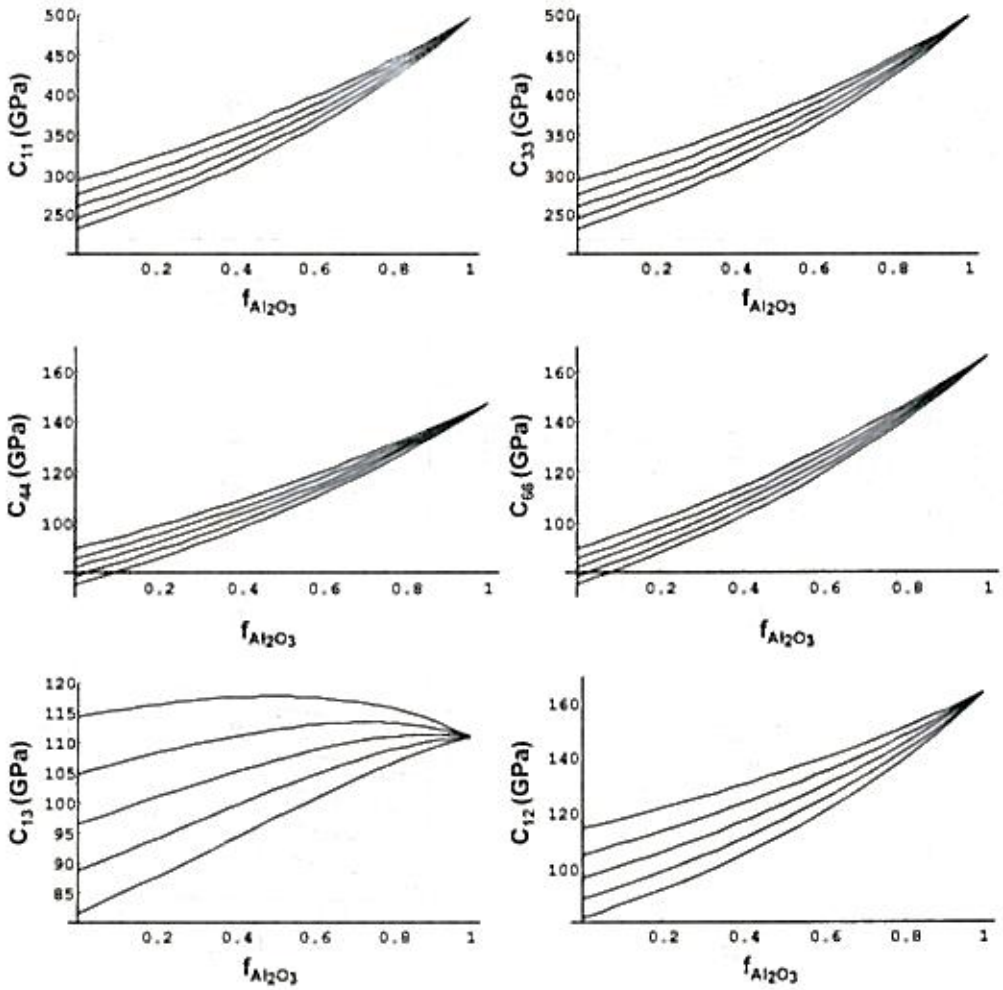

Fig. 7. Companion to Fig. 6 covering the entire composition range. See Fig. 6 caption for curve identification.

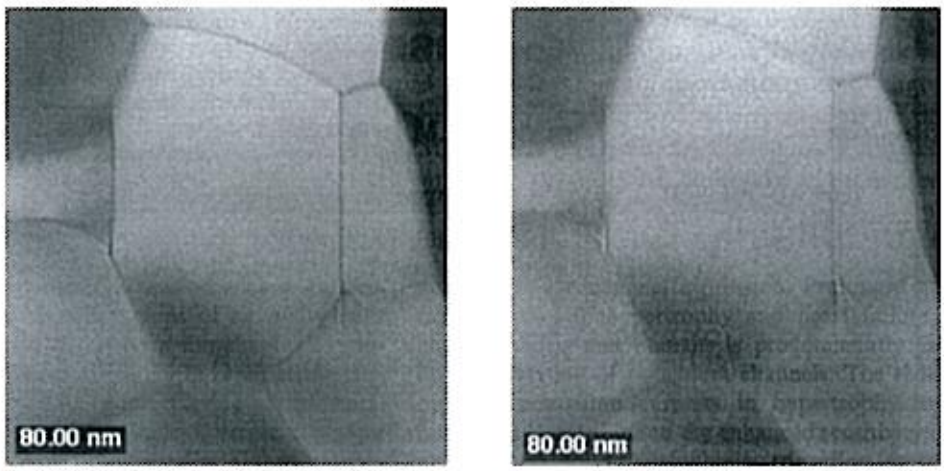

Fig. 8. Images of mullite–mullite boundaries. Dark fringe in over-focus image (left) and bright fringe in under-focus image (right) indicate an intergranular phase.

same silica fraction is required for all six C_{ij} supports the validity of the calculation and the basic hypothesis of silica enveloping the mullite particles.

To avoid the impression that the C_{ij} change linearly with alumina concentration, Fig. 7 shows the entire volume-fraction range. Except for the C_{13} case, all predicted curves show the usual concavity. The C_{13} curve is convex because of the microstructure: platelets aligned perpendicular to x_3. The C_{23} curve (not shown) is identical to the C_{13} curve.

Encouraged by the solid-mechanics-calculation results, we then looked carefully for physical evidence of silica at mullite–mullite boundaries. Specimens for TEM and STEM were obtained by conventional methods. The general microstructural features were examined in an electron microscope, and Fresnel imaging was used to identify the presence of intergranular phase. The chemical composition of the intergranular phase was obtained on a VG HB5 dedicated STEM with a 1-nm probe size and an EDS detector.

The specimen was very dense with no small amorphous pockets at multiple grain junctions, as shown in Fig. 8: the Fresnel images of the mullite matrix showing connected (or enveloped) intergranular phase. The presence of a dark fringe in the over-focus image and a bright fringe in the under-focus image between mullite grains indicates that there is an intergranular phase between mullite grains. This kind of intergranular phase was always observed whenever the grain boundaries in the mullite matrix were tilted parallel to the electron beam. Fig. 9 shows two EDS spectra obtained from the mullite grain and from the intergranular phase by using STEM with a 1-nm probe. The mullite grain has an Al:Si ratio of about 3:2, whereas the intergranular phase has an Al:Si ratio of about 5:7. Thus, our hypothesis was confirmed that the presence of a silica-rich, enveloping, soft phase around mullite grains causes an elastic softening of the composite. No intergranular phase was

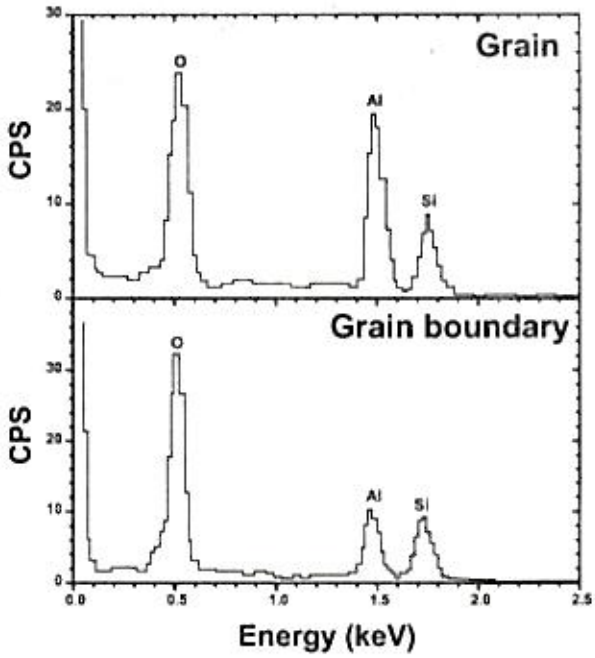

Fig. 9. Energy-dispersive-spectroscopy spectra of mullite grain and intergranular region showing silica-rich regions near grain boundaries.

detected in the mullite–alumina grain boundaries. However, the small volume fraction of grain-boundary silica must also bond poorly with the adjacent mullite grains to explain the large elastic softening.

5. Conclusions

The measured elastic stiffnesses of alumina-platelet-reinforced mullite-matrix composites fall far below the expected values predicted by simple solid-mechanics-theory calculations. Considering all the usual elastic-softening sources, we concluded that the mullite grains must be enveloped by a soft (probably glassy) silica

phase. Careful solid-mechanics-theory calculations supported this conclusion. Careful searching using TEM and STEM methods confirmed silica-rich grain-boundary regions. The small volume fraction of these silica regions suggests that the silica–mullite bonding is much weaker than the mullite–mullite bonding.

Acknowledgements

The study at the University of Illinois (Frederick Seitz Materials Research Laboratory, Center for Microanalysis of Materials) was supported by the US Department of Energy under contract DEA-CO2-76ER0-1198.

References

1. Schneider, H., Okada, K. and Pask, J., *Mullite and Mullite Ceramics*. Wiley, Chichester, UK, 1994.
2. Aksay, I. and Pask, J., Stable and metastable equilibria in the system SiO_2–Al_2O_3. *J. Am. Ceram. Soc.*, 1975, **58**(11–12), 507–512.
3. Maynard, J., Resonant ultrasound spectroscopy. *Phys. Today*, 1996, **49**, 26–31 (Jan.).
4. Migliori, A. and Sarrao, J., *Resonant Ultrasound Spectroscopy*. Wiley, New York, 1997.
5. Ledbetter, H., Fortunko, C. and Heyliger, P., Orthotropic elastic constants of a boron–aluminum fiber-reinforced composite: an ultrasonic-resonance-spectroscopy study. *J. Appl. Phys.*, 1995, **78**, 1542–1546.
6. Ledbetter, H., Kim, S., Fortunko, C. and Heyliger, P., Compressibility of polycrystal and monocrystal copper: acoustic-resonance spectroscopy. *Int. J. Thermophys.*, 1996, **17**, 213–269.
7. Bhatia, A., *Ultrasonic Absorption*. Oxford, London, 1967 (p. 330).
8. Ledbetter, H. and Datta, S., Effective wave speeds in an SiC-particle-reinforced Al composite. *J. Acoust. Soc. Am.*, 1986, **79**, 239–248.
9. Ledbetter, H., Datta, S. and Dunn, M., Elastic properties of particle-occlusion composites: measurements and modelling. *J. Eng. Mater. Technol.*, 1995, **117**, 402–407.
10. Dunn, M. and Ledbetter, H., Elastic constants of composites reinforced by multiphase particles. *J. Appl. Mech.*, 1995, **62**, 1023–1028.
11. Ledbetter, H., Kim, S., Crudele, S. and Kriven, W., Elastic properties of mullite. *J. Am. Ceram. Soc.*, 1998, **81**(4), 1025–1028.
12. Tefft, W., Elastic constants of synthetic single-crystal corundum. *J. Res. Nat. Bur. Stand.*, 1966, **70A**, 277–280.
13. Dunn, M. and Ledbetter, H., Poisson's ratio of porous and microcracked solids: theory and application to oxide superconductors. *J. Mater. Res.*, 1995, **10**, 2715–2722.
14. Hill, R., A self-consistent mechanics of composite materials. *J. Mech. Phys. Solids*, 1965, **13**, 212–222.
15. Dvorak, G., Plasticity theories for fibrous composite materials. In *Metal Matrix Composites, Mechanisms and Properties*, Vol. 2, ed. R. K. Everett and R. J. Arsenault. Academic Press, Boston, 1991, pp. 1–77.
16. Mori, T. and Tanaka, K., Average stress in matrix and average elastic energy of materials with misfitting inclusions. *Acta Metall.*, 1973, **21**, 571–574.
17. Eshelby, J., The determination of the elastic field of an ellipsoidal inclusion, and related problems. *Proc. Roy. Soc. Lond.*, 1957, **A241**, 376–396.
18. Mura, T., *Micromechanics of Defects in Solids*, 2nd edn. Martinus Nijhoff, Dordrecht, 1987.